RSC Advances




ROYAL SOCIETY OF CHEMISTRY

www.rsc.org/advances

# Preparation, characterization and application of Antibody-Conjugated Magnetic Nanoparticles in the Purification of Begomovirus

**Michael Immanuel Jesse[a], R. Sukanya[b], D.Nallusamy[a], T.Raja Muthuramalingam[a], S.U.Mohammed Riyaz[a], G.Dharanivasan[a], K.Kathiravan*[a]**

[a]Department of Biotechnology, University of Madras, Guindy, Chennai – 600 025, Tamil Nadu, India.

[b]Department of Bioscience & Biotechnology, Banasthali University, Rajasthan – 304022, India.

*Corresponding author

email: drkkathiravan@gmail.com. Tel : +91 44 2220 2744

**Keywords**

Begomovirus, Magnetic nanoparticles, Antibody, Bio-separation, Electrophoresis.

## ABSTRACT

Begomovirus (family-*Geminiviridae*) infect a wide range of commercial crops like tomato, bean, cassava, cotton, cucurbits and chilli. Purification of begomoviruses from the infected plants, in particular from vegetable crops remains challenging. The conventional process of begomovirus purification requires sophisticated instruments and moreover, it is time-consuming. Herein, we used antibody-conjugated magnetic nanoparticles (Ab-MNPs) to purify begomoviruses from the infected plants. MNPs were prepared using the co-precipitation method (at pH between 8-12 & size 25nm). The prepared MNPs were functionalized with APTES (at pH 7) and confirmed with FTIR. Thus functionalized MNPs were conjugated with polyclonal antibodies (pAbs) using the EDC-NHS chemistry (size = 80nm). The crude extract prepared from the infected plants were suspended in the solution of Ab-MNPs and separated using a magnet. The captured virus particles were released into the aqueous solution (at pH 10). SDS-PAGE analysis and PCR analysis were done to confirm the presence of viral infection.

## Introduction

Researchers show great interest from the wide range of applications of magnetic nanoparticles (MNPs) in the following disciplines including magnetic fluids,[1] catalysis,[2,3] biotechnology/biomedicine,[4] magnetic resonance imaging,[5,6] data storage[7] and environmental remediation.[8,9] The successful application of magnetic nanoparticles in various areas of research is highly determined by their stability. The common methods for the synthesis of magnetic nanoparticles include co-precipitation, Thermal decomposition, hydrothermal synthesis, micro-emulsion, sonochemical synthesis[10] and other methods involved are electrochemical synthesis,[11] laser pyrolysis technique[12] and microorganism/bacterial synthesis.[13] Among these techniques, co-precipitation is considered to be facile and efficient way to synthesize MNPs. Based on the reaction between the ferric and ferrous ions at the molar ratio of 1:2 combined with high pH, ionic strength and nitrogen bubbling contributes to the decrease in the size of the nanoparticles.[14,15] The $Fe_3O_4$ is expected to be synthesized between pH 8 to 14.[15] Further, dispersion of MNPs could be achieved through different strategies of bio-functionalization. The magnetic nanoparticles that are below 100 nm diameter possess a large surface area, lower sedimentation rates and improved tissular diffusion[16,17,18] and the dipole-dipole interactions are significantly reduced due to their r6 scale is another advantage[19]. It is due to their small size and high surface area, magnetic nanoparticles have distinct characteristics of their application in bioseparation compared to the conventional commercially available microbeads. The characteristics such as their good dispersibility, rapid and efficient binding of biomolecules and reversible/controllable flocculation.[20]

The deep understanding and knowledge on the bio-functionalizing moieties and their interstellar distribution on the nanoparticle surfaces favors the functionalization of biomolecules. Bare MNPs possess certain limitations that it is unstable in strong acidic solution and tend to undergo leaching thereby reducing its reusability and lifetime. In the absence of appropriate functional groups, the hydrophobic surfaces on bare MNPs tend them to form agglomeration. Such limitations would make these MNPs unsuitable for immobilization of proteins and peptides. Therefore, functional groups including silanes, carboxylates and diols have been known to demonstrate surface modification strategies of metal nanoparticles like magnetite and maghemite.[21] Various surface modification strategies have been developed to

renovate the hydrophobic iron oxide nanoparticles to hydrophilic particles using biocompatible coating materials, biomolecules and hydrophilic small molecules.[22] Several surfactants including oleic acid, lauric acid, alkylsulphonic acids, and alkylphosphonic acids have been used.[23] Polyethylene glycol (PEG), polyvinylpyrrolidone (PVP), poly(ethylene-co-vinyl acetate), poly(lactic-co-glycolic acid) (PLGA), and polyvinyl alcohol (PVA) are the polymers that have been used.[24] Natural dispersants including gelatin, dextran, polylactic acids, starch, albumin, liposomes, chitosan, ethyl cellulose have also been extensively employed for coating purpose in aqueous medium. Silanization is the most widely used technique to functionally modify the surface of bare magnetic nanoparticles due to its characteristics such as satisfying responsivity, low cytotoxicity, high stability under acidic conditions, inertness to redox reactions and easy to perform surface chemical modification. Their ability to react in either aqueous media or organic solvents at moderate temperatures under moderate conditions makes the silanization strategy ideal for surface functionalization.

The silane molecules are activated by the process of hydrolysis following which condensation occurs between Si-OH groups of the silanol and the hydroxyl groups on the MNP surface forming stable bonds on the surface.[25] The bio-functionalized magnetic nanoparticles have enormous interest due to their wide use in the field of biotechnology and bio-nanomedicine.[26,27] Bio-functionalized magnetic nanoparticles have been aided in the immobilization of biological materials including low molecular weight ligands, peptides, proteins, polysaccharides, polyunsaturated fatty acids, DNA, plasmids, siRNA etc.[28] The conjugation of antibody to nanoparticles make them 'super-recognizers' that could specifically target antigen of interest.[29]

The wide applications of antibody-conjugated magnetic nanoparticles include therapeutics, diagnostics and bio-separation. Antibody-conjugated magnetic nanoparticles (Ab-MNPs) are widely used in [1] targeting and treatment of various cancers,[30,31] [2] magnetic resonance and imaging,[32,33] [3] Hyperthermia[34] and [4] magnetic separation, purification and immunoassay.[35] Magnetic bio-separation is the recently developing area in the field of nano-biotechnology which could slowly deteriorate the use of sophisticated, expensive instruments such as ultra-centrifuges used for separation. The applications of magnetic nanoparticles in the bio-separation techniques can solve different problems including high-cost and process

complexion.[36,37,38] The significant ability of bio-moiety (antibody) functionalized iron oxide nanoparticles in bio-separation will gain greater interests of industrial community in the separation of target molecules. Magnetic bio-separation possesses certain advantages such as 1) their ability to recover small particles (0.05 - 1μm) in the presence of multi-components or biological debris,[39] 2) efficiently applicable for large-scale purification, 3) allows to save more time and money,[38] 4) centrifugation steps can be avoided and 5) cross-contamination could be avoided. The antibody-conjugated iron oxide nanoparticles have been employed in the separation of cancer cells,[39] pathogens including *E.coli* and *Staphylococcus*[42] and CD3+ T-cells,[43] in addition, magnetic separation and immunoassay on multi-antigen system[44] have been demonstrated. Some of the major advantages of employing nanoparticles as platform for functionalization of biomolecules are 1) their small size, 2) High surface area, 3) Modification using functional groups increasing its high capacity or selectivity and greater stability during storage.

In this study, we have demonstrated the magnetic bio-separation of Begomovirus from the infected plant samples. Begomovirus is considered to be a largest and most vital genus that belongs to the family *Geminiviridae*. These viruses tend to infect mostly dicotyledonous plants. These damaging plant viruses show severe threat to global food security. The symptoms of virus infection in plants are leaf curling, mosaic, vein yellowing and stunting of plant growth.[45,46,47] These viruses are transmitted by white-flies (*Bemisia tabaci*). These are single-stranded DNA viruses that possess icosahedral twinned geminate particles. The transmission of these viruses by insects are mostly dependent on the coat protein that are adapted to different receptors of insects.[45] In 1998, Swanson et al. has made the epitope profiles and antigenic properties of Begomovirus coat protein within genus. Swanson et al (1988) used both monoclonal antibodies and polyclonal antibodies for epitope profiling on the coat protein of Begomovirus.[48]

Here in, we have conjugated the polyclonal antibodies (pAbs) specific to the genus Begomovirus on the surface of iron oxide nanoparticles for its bio-separation from the symptom showing squash plants *Benincasa hispida* for which we have reported the incidence of *Squash Leaf Curl China virus* (SLCCNV), a species of begomovirus.[49] So far, conventional methodologies like ultra-centrifugation that are very expensive and time-consuming, have been used for the separation and purification of

Begomovirus from the debris.[50] We demonstrate a low-cost, time saving purification technique that employs antibody-conjugated magnetic nanoparticles in the purification of begomovirus from the infected plant. This technique of employing iron oxide nanoparticles for the separation/purification of begomovirus from the infected ash gourd (*Benincasa hispida*) plant samples would skip the centrifugation process with the great power of magnets.

## Material and Methods

### Materials

All reagents used for the synthesis of iron oxide nanoparticles were analytical grade purchased commercially and used as received. Ferrous chloride hydrated extra pure (code no. 03846) and Ferric chloride anhydrous 98% extra pure (code no. 03817) were obtained from Loba Chemie Pvt. Ltd. Sodium Hydroxide pellets were obtained from RANKEM (code no. S0270). Sodium hydrogen phosphate –monobasic (1949146) and dibasic (1949144), Sodium lauryl sulphate (1948101), Tris buffer (2049171), Acrylamide, Bis-acrylamide, TEMED and APS were purchased from Sisco Research Laboratories Pvt. Ltd. APTES (154766) was obtained from MP biomedicals. Hydrochloric acid was purchased from Merck and nitric acid from Fisher Scientific India Pvt. Ltd. Ultrapure Milli-Q water was used throughout the study (Millipore). Aqua regia was freshly prepared for washing glasswares used for the synthesis of iron oxide nanoparticles.

### In situ precipitation of iron oxide nanoparticles modified with APTES

Magnetic nanoparticles were synthesized with modifications on the previously demonstrated protocols[51-57] through co-precipitation of ferrous and ferric salts under the presence of $N_2$ gas with the help of NaOH solution. 16.25g of $FeCl_3$ and 6.35g of $FeCl_2$ were dissolved in 200 ml of distilled water, which leads to $Fe^{2+}/Fe^{3+}$ ratio of 2:1 in the solution. The nitrogen gas provides an inert atmosphere, thereby preventing the oxidative conversion of magnetite to maghemite particles. The solution was stirred for 1 h at 30ºC. The co-precipitation reaction has taken place by raising the pH of the

solution to 12 by adding 2M NaOH drop-wise into the reaction system at 70ºC. The reaction was sustained for 3 hours at 70ºC with the continuous supply of nitrogen gas.

The following reaction occurs during the synthesis process.

$$2FeCl_3 + FeCl_2 + 8NaOH \rightarrow Fe_3O_4\ (s) + 4H_2O + 8NaCl$$

After the completion of the reaction, the synthesized particles were cooled down and washed with double deionized water. The particles were repeatedly washed with the deionized water to remove excess of NaOH which was done till the pH reaches 6-7. According to Laconte et al (2005), the as-of synthesized magnetic nanoparticles aggregated due to the van der Waals forces resulting in the increase in the size of the particles[16]. The black precipitate was sonicated for separating the particles for further modification. The particles were surface modified with the silanization process. 80 ml of 10% APTES was added drop-wise to ferro-fluid suspension under constant stirring. Before addition, the pH of the APTES solution was adjusted to 4 using glacial acetic acid. The reaction content was vigorously stirred for 1 h in nitrogen atmosphere. The particles were thoroughly washed with double deionized water through continuous collection and dispersion process (magnetic decantation) until the solution reached neutral pH. A small amount of precipitate was dried in a vacuum dessicator.

**Conjugation of Antibodies to the APTES-MNPs**

The antibody was conjugated on the magnetic nanoparticles based on the following protocol. The antibody was conjugated to the magnetic nanoparticles in 1:200 dilution. 10mM EDC and 5mM NHS were prepared in 0.1 M MES buffer at pH 5 and incubated with anti-ACMV antibody in a humid chamber for 1 h. Then 20µl of EDC-NHS activated antibody solution was added to MNP solution. Following which 20µl of 10mM phosphate buffer was added to 980µl of reaction solution. The reaction mixture was incubated for overnight at 30ºC in vortex mixer. Antibody-conjugated MNPs were separated by placing the tube in a magnet. The pellet was collected and re-suspended in PBS for washing. Totally three washing steps were done and finally suspended in PBS.

**Field survey and collection of squash plants showing begomovirus-infection symptoms**

The squash plants *Benincasa hispida* showing symptoms of begomovirus infection was collected. Upon begomovirus infection, the plants develop symptoms including leaf curling, mosaic, vein yellowing or stunting of plant growth. The plant leaf samples showing such symptoms were collected from the nearby areas of Thiruvallur district. The inhabitation of white-flies (*Bemisia tabaci*) on the leaves also ensured Begomovirus infection.

**Extraction of DNA from infected plant leaves**

Total Genomic DNA was extracted from the symptomatic squash leaf samples using protocol suggested by Dellaporta et al. in 1983. Two leaf discs from collected leaf samples were taken in a sterile eppendorf tube (1.5 ml) and ground with 700 µl of Dellaporta buffer using a micro pestle.[58] 100 µl of 10% SDS was added into the tube and mixed well and incubated at 65ºC for 10 minutes using a water bath. This was followed by addition of 200 µl of 5 M potassium acetate and vortexing for 5 minutes. The sample tubes were then incubated in ice for 20 minutes. Afterwards, the tubes were centrifuged at 10,000 rpm for 15 minutes and supernatant was collected in a fresh eppendorf tube and equal volume of isopropanol was added, the tubes were then vortexed and incubated at -20ºC for 30 minutes. After the incubation, the tubes were centrifuged at 10,000 rpm for 10 minutes and supernatant was discarded. To the remaining pellet, 70% ethanol was added and again centrifuged at 10,000 rpm for 15 minutes. Supernatant was discarded and pellet was dried completely before addition of 50 µl distilled water and storage at -20ºC.

**Confirmation of begomovirus infection using conventional techniques**

The infection in squash plants was confirmed using polymerase chain reaction (PCR) through selective amplification of coat protein gene. The primers specific to the *CP* gene of *Squash leaf curl China Virus* were used for the validation. The following

reactions mixture was prepared: 0.5µl nuclease free water, 5µl master mix, 0.25µl forward primer, 0.25µl reverse primer, 4µl extracted total DNA solution.

**Extraction of filtrate from squash plant leaves**

The plant leaf extract was prepared through filtration method. The symptomatic leaves (100 g) were washed in water and kept in -20ºC overnight. The frozen leaves were then homogenized by 0.1 M Phosphate buffer using mortar and pestle. The plant extract was filtered through No.1 Whatmann filter paper.

**Immunopurification of virus particle using antibody-MNP conjugates**

The Ab-conjugated MNPs solution was taken in five tubes in equal volume. 25µl, 50 µl, 75 µl, 100 µl and 125 µl of crude extract was added to the tubes followed by incubation at RT for 30 mins. Afterwards, coupling buffer at pH 7.0 was added and incubated for 1 h. The Ag-Ab-MNP complex was separated using a magnet and washed 3 times with washing buffer. This complex was later suspended in 200 µl of Antigen Retrieval buffer (ARB) at RT for 30 mins and kept under vortex.[59] The virus particle i.e. the antigen was purified from the debris.

**Results and discussion**

Iron oxide nanoparticles were prepared using a modified protocol of so far available co-precipitation method[14,15]. The $Fe^{2+}$ and $Fe^{3+}$ salts were co-precipitated using sodium hydroxide to form magnetite.

**In situ preparation of iron oxide nanoparticles modified with APTES**

Magnetite nanoparticles was synthesized using the modified co-precipitation method described previously. Fe(II) and Fe(III) salts were co-precipitated using the aqueous NaOH solution. The stoichiometric ratio of $Fe^{3+}$ to $Fe^{2+}$ was set to 2:1 in the solid phase at the pH range between 10 – 12 at 70ºC. The reaction was carried out under the

continuous supply of Nitrogen gas. The co-precipitation method using $Fe^{2+}$ and $Fe^{3+}$ ions reacting in alkaline conditions has been extensively investigated and the following reactions were proposed for the mechanism of magnetite formation:

$$Fe^{3+} + 3OH^{-} = Fe(OH)_3\ (s)$$

$$Fe(OH)_3\ (s) = FeOOH\ (s) + H_2O$$

$$Fe^{2+} + 2OH^{-} = Fe(OH)_2\ (s)$$

$$2FeOOH\ (s) + Fe(OH)_2\ (s) = Fe_3O_4\ (s) + 2H_2O$$

Giving an overall reaction:

$$2Fe^{3+} + Fe^{2+} + 8OH^{-} = 2Fe(OH)_3Fe(OH)_2\ (s) \rightarrow Fe_3O_4\ (s) + 4H_2O$$

The reaction was carried out in Nitrogen atmosphere because magnetic nanoparticles has the tendency to become maghemite[60] due to its instability and susceptibility to oxygen. This can be represented by the following equation.

$$Fe_3O_4 + 0.25O_2 + 4.5H_2O \rightarrow 3Fe(OH)_3$$

$$Fe_3O_4 + 2H^{+} \rightarrow \gamma Fe_2O_3 + Fe^{2+} + H_2O$$

Thus prepared magnetite nanoparticles possess a net negative charge due to the $-OH^{-}$ ions on their surface. The inter-particle distance therefore get decreased and tend to come closer to each other causing aggregation of particles thus resulting in the increase in the particle size.[61,62,63,64,65] The poly-dispersity among the particles makes it unsuitable for bio-applications.[66] In order to overcome such problems, the surface of iron oxide nanoparticles were coated with appropriate functional moiety. Certain parameters were considered while choosing a suitable functional moiety: 1) the stability of the surface coat, 2) type of biomolecule to be conjugated, 3) side chain chemistry of the biomolecule, 4) dispersity of nanoparticles and 5) redox potential. Upon functionalization with suitable capping agent, the nanoparticles stay apart from each other due to the steric/electrostatic repulsion between particles. Here in, we demonstrated the conjugation of anti-ACMV antibody on the surface of iron oxide nanoparticles. Generally, antibody possess two ends: variable end and constant end. The variable end inhabits most of the amino ($-NH_3^{+}$) groups and the latter is known to possess carboxyl groups. Therefore bio-conjugation was done using the $-COO^{-}$ end groups of the antibody which do not affect the specificity of the antibody. In order to build a covalent linkage between the nanoparticles and antibody APTES was used as coating compound. Upon encapsulation with APTES, the surface of the nanoparticles were left positive. The following analyses were carried out for the physico-chemical

characterization of magnetic nanoparticles: Transmission electron microscopy, Particles size analyzer (DLS), Surface Charge Analysis (Zeta-sizer), X-ray diffraction (XRD), Fourier Transform Infrared Spectroscopy (FT-IR), Vibrating Sample Magnetometer (VSM) and UV-Visible Spectrophotometer.

## Characterization of APTES modified iron oxide nanoparticles

### Particle size analyzer

The size distribution of the magnetic nanoparticles was determined using Malvern Nano ZS Zetasizer. The size of the magnetic nanoparticles determined using the multiple scattering techniques through laser diffraction method was approximately from 10 to 100nm. The average diameter of the APTES-functionalized magnetic nanoparticles (APTES-MNPs) was ~25nm (Fig. 2a).

The particle size is the main factor that makes the particle suitable for various applications. Especially, the particles can be used for biomedical applications only at smaller size.[67] It has been known that the particle size of the particles depends on the acidity and the ionic strength of the medium.[13,68] The particle size decreases at higher pH and ionic strength. The chemical composition on the surface of the particles and consecutively, the surface charge of the particles are determined by the pH and the ionic strength of the medium. Another factor that influences the particle size is the mixing rate of the solution. As the mixing rate increases the size of the particles tend to decrease. The limit of oxidation rate is also factors influencing the particle size. It has been proved that bubbling of medium with nitrogen decreases the particle size when compared to the methods without oxygen removal.[69,70] The particle size is also dependent on the proportion of the iron salts used for the preparation of iron oxide nanoparticles.[71]

### Surface Charge Analysis

The surface charge or the zeta potential ($\zeta$) of the magnetic nanoparticles was analyzed in Malvern ZS Nano instrument using laser Doppler velocimetry technique. The APTES-MNPs exhibited positive charge of around +25mV at <pH 10 which is essential for an ideal electrostatic stabilization. The surface charge of the particles is positive due to the silane molecule APTES that has been coated on the surface of the

magnetic nanoparticles at neutral pH[72] indicating that all the $-NH_2$ groups have been transformed to $-NH_3^+$ group. The surface charge was determined by the pH of the solution. Since the silanization process was carried out in neutral pH, the zeta potential was taken at pH 6.8. The electrostatic repulsion between the particles is based on the surface charge of the particles. The net positive charge of the particles makes the particle repel each other. The repulsion force between particles has prevented them from aggregation maintaining mono-dispersity.[21] (Fig. 2b). Therefore, surface bio-functionalization of magnetic nanoparticles is a most important step to prepare stable particles in the medium. A net positive charge is most vital for the covalent immobilization of antibody on the magnetic nanoparticles. The result proves that the particles are stable in the medium at neutral pH.

**Fourier Transform Infra-red spectroscopy (FT-IR)**

The coating of the magnetite surface through silanization was confirmed using FTIR spectroscopy. Fig. 2c shows the FTIR spectra of the MNPs and APTES-MNPs. For MNPs nanoparticles, the characteristic absorption peaks at 601 and 702 $cm^{-1}$ are attributed to the Fe-O stretching in the (*a*-*b*) plane.[73] APTES is adsorbed on the magnetite nanoparticles surfaces by Fe-O-Si bond, because of the absorption band corresponded to this band appears at around 601 $cm^{-1}$ and therefore overlaps with the Fe-O bend, while Si-O stretching was observed at 987.48 $cm^{-1}$.[74] The band at 1319.2 and 1396.36 $cm^{-1}$ corresponds to C-O stretch and C-H bend, respectively. The IR absorbance at 1650.94 $cm^{-1}$ corresponds to the stretching vibration at N-H bend which is a primary amine, $NH_2$ groups, confirm the existence of APTES. Finally, the weak FTIR peak at 3618.1 $cm^{-1}$ relates to the free O-H groups concerned with surface exposed MNPs. Therefore, the presence of Fe-O bend, Si-O stretching, and N-H bend provide evidence for APTES being functionalized on the surface of MNPs.

**X-ray Diffraction Techniques**

The XRD data revealed typical X-ray powder diffraction patterns of magnetite nanoparticles at pH 7 (Fig. 2d). The structural and phase investigation of samples are analyzed by XRD measurements which have been compared with the standard data at the solution with pH 7. There are no significant existence of other phase or impurity. It was found that the samples showed crystalline and strong orientation at (220), (311), (400), (422), (511) and (440) planes with $2\theta$= 30.0º, 35.4º, 43.0º, 53.4º, 56.9º

and 62.5º, respectively. There are no intense peaks along (110), (210), (211) that are corresponding to γ–$Fe_2O_3$ particles.[68,75] The crystalline grain size was determined using Debye-Scherrer Equation D= 0.9λ/ ($\beta$cosθ) for intense peak. The calculated average size of the nanoparticles calculated from XRD studies is 14.05nm. The fact, based on the Ostwald ripening theory,[76] the precipitated particles possesses larger crystalline sizes due to the high pH and the increased temperature. After surface modification, the particles become smaller due to the inter-particle repulsion force. Comparatively, small particles are preferred for their higher surface energy.[68]

**Vibrating Sample Magnetometer**

The characterization of the magnetic properties of the $Fe_3O_4$ nanoparticles was done using vibrating sample magnetometer (VSM) at room temperature thereby cycling the magnetic field between -15000 to +15000 $O_e$, where parameters such as saturation magnetization ($M_s$) and coercive field ($H_c$) were evaluated. Hysteresis curves of the magnetic nanoparticles in powder state was measured (Fig. 2e). The nano-fluidic behavior of the magnetite nanoparticles was mainly determined by their magnetic properties. It has been known that in the existence of magnetic field H, the magnetic moment (μ) of the particles will tend to arrange along the magnetic field direction, leading to a macroscopic magnetization of the liquid. These type of magnetic materials show hysteresis loops (M-H curves) which could be defined by the irreversibility in the magnetization process related to the pinning of magnetic domain walls at impurities or crystal defects which often restricts the domain wall motion. Another potential cause of such a behavior is the magnetic anisotrophy of the crystalline lattice. With the increase in the applied field, the domains change size and rotate until the materials gets fully magnetized leading to the saturation magnetization ($M_s$). The magnetic moment of the particle freely oscillate with respect to the heat energy. Thus obtained saturation magnetization, $M_s$ and coercive field, $H_c$ at room temperature were 14.5 emu/g. It has been suggested that $M_s$ of nearly 7-22 emu/g is found suitable for biomedical applications.[77,78] The decrease in the size of the magnetic nanoparticles results in the decrease of saturation magnetization which is due to the large deformations occurred on the surface of small particles. The mean magnetic diameter ($D_{mag}$) and the standard deviation, σ calculated based on the low field and high field portions at room temperature using Chantrell's equation.[68,79] Thus synthesized APTES-MNPs found suitable for the application of virus purification.

**Bio-functionalization of antibody on magnetic nanoparticles**

In order to immobilize protein molecules, the side chain of protein of interest has to be activated with suitable linker and the nanoparticles as well. The purpose of surface activation of $Fe_3O_4$ nanoparticles was solved by coating the nanoparticles with APTES to form self-assembled monolayers on the surface of these magnetic nanoparticles. The side chain carboxylic group of the antibody molecule was activated by EDC-NHS strategy.[80]

There are two methods so far to immobilize antibody on nanoparticle surface; Non-oriented binding and Oriented Binding. In non-oriented binding, the antibodies are directly immobilized on the surface of the magnetic nanoparticles, the most common method that applies ionic based interaction between the antibody and nanoparticle complex. This type of immobilizing antibodies on magnetic nanoparticles may disturb the coupling efficiency of antibody to the antigen either due to the steric restrictions or the blocking up of reactive sites that aids in the specificity of the molecule. Therefore, specificity of antibody can be increased only through 'targeted binding' or the 'oriented binding' approach achieved by the covalent immobilization of magnetic nanoparticles to the Fc domain in the antibody[81].

The amount of antibody loaded on the surface of the magnetic nanoparticles were measured using Bradford assay. The calibration curve was obtained from the absorbance derived at 595nm (data not shown). The antibody concentration was measured in the sample tube before and after conjugation to magnetic nanoparticles. The amount/percentage of surface bound protein on the magnetite nanoparticles was calculated from the residual protein left out in the sample tube after bio-functionalization. The percentage of antibody loaded could be calculated using the following formula:

$$\text{Percentage of Antibody (\%)} = \left(\frac{\text{Initial Concentration of Antibody} - \text{Final Concentration of antibody}}{\text{Initial Concentration of Antibody}}\right) \times 100$$

In such a way, it was found that nearly 75% of the antibody molecules were immobilized on 1 mg of magnetic nanoparticles, i.e. the given initial concentration of antibody was 1.2 mg/mL and the final quantity of antibody left in the sample tube was

0.35 mg/mL (Fig. 3b). The high percent of loading of antibody on the surface of the magnetic nanoparticles is due to the activation of the carboxyl group in the antibody at a slightly acidic pH.[82] Further the Ab-MNPs were characterized using particle size analyzer. The antibody-conjugated magnetic nanoparticles showed a drastic change in their size compared to bare MNPs which might be due to the surface capping of the nanoparticles by the antibody.

It is because of the polymeric nature of the antibody the magnetic nanoparticles come close together to increase the size of the particles. Thus measured size of the particles was ~80nm in diameter (Fig. 3a). This result clearly indicates that the hydrodynamic diameter of the particles has increased due to the agglomeration of particles caused by antibody.

**Bio-Separation of Begomovirus using Ab-MNPs**

The Ab-MNPs were used to precipitate the virus particles from the solution. The antibody-conjugated magnetic nanoparticles aggregated due to the adhered virus and the formed hydrogen bonding in between the viral antigen and the antibody. The increase in the size of the magnetic nanoparticles were measured using the particle size analyzer (Fig. 4a).

The hydrodynamic diameter of the nanoparticles increased to nearly 1100 nm i.e. 1.1 μm which confirms the immunoprecipitation complex in between the magnetic nanoparticles. SDS PAGE analysis for the solution eluted from the first wash was run along with the partial purified sample (Fig. 4c). In gel lane 1, the separated crude extract sample has found to possess multiple protein bands. It is clearly understood that the appeared multiple protein bands was due to the presence of enormous plant proteins. This has been further proven by UV-Visible spectrophotometer (Fig. 4b), which exhibit peak at 265 nm indicating the presence of biomolecules, i.e. DNA/proteins. The amplification of CP gene in the crude extract indicates the presence of viral infection (control). But the CP gene was not amplified in MNPs treated samples (Fig. 4d). This clearly indicates that huge amount of virus particles have adhered to the antibody immobilized magnetic nanoparticles. During the second wash and the third wash, the virus particles were not found. The antigen-antibody-MNP aggregates were suspended to antigen retrieval buffer (ARB) at pH 10. The ionic strength of the solution plays an important role in the release of captured

antigen. It is also due to the fact that surface charge of the virion particles becomes zero at that particular pH. After incubation with ARB, the antigen was released from the Ab-MNPs complexes and left free in the medium. The remaining Ab-MNP conjugates were separated using the magnet. The release of antigen in the solution was confirmed using the SDS-PAGE electrophoresis, PCR and Agarose gel electrophoresis. The SDS-PAGE showed intact bands between 56 kDa and 101 kDa, at ~85 kDa which should be a trimer of the 28.6 kDa coat protein of begomovirus (Fig. 5a)[83]. The isolated viral particles were compared with the viral particles extracted using the conventional techniques and the Ab-MNPs recycled to isolate viral particles in a sample (Fig. 5b). Therefore, it confers that these Ab-MNPs can be reproduced rather than get wasted. The presence of proteins was further confirmed using UV-Visible spectrophotometer as the absorbance peak was found at ~270nm (Fig. 5c). The broad peak at 400nm decreased indicating the reduction in the Ab-MNP complex. The CP gene was amplified using polymerase chain reaction in all the samples confirming the presence of virus particles (Fig. 5d). The antibody conjugated magnetic nanoparticles was more helpful in the purification of virus particles skipping the most expensive ultra-centrifuge technique. This technique employing the use of magnetic nanoparticles would help the research community in the bioseparation/purification of virus particles using a magnet.

## Conclusions

This work reports for the first time about the powerful application of antibody conjugated MNPs in the purification of begomovirus from the infected plant samples. The hydrophobically prepared magnetic nanoparticles were modified into hydrophilic particles using APTES mediated silanization. APTES modified MNPs showed a mean diameter of ~25nm. Thus synthesized APTES-MNPs was conjugated with the antibodies specific for Begomovirus. The antibody-conjugated MNPs was found to be ~80nm in diameter due to the surface coverage with antibodies. While Ab-MNPs were suspended in the crude extract of ash gourd leaf samples, the Ab-MNPs has acquired the viral antigens through immunoprecipitation reaction resulting in a drastic increase in diameter i.e. 1100nm which were then separated using a magnet. Finally, after treating with Antigen retrieval buffer at pH 10, the captured virion particles are released into the buffer solution. The results were confirmed using SDS-PAGE,

490 Polymerase Chain reaction and agarose gel electrophoresis. This technique will serve
491 as a great tool for researchers to skip off the time-consuming ultra-centrifugation step
492 for the separation of biomolecules.

493

## References


(1). S. Chikazumi, S. Taketomi, M. Ukita, M. Mizukami, H. Miyajima, M. Setogawa, Y. Kurihara, Physics of magnetic fluids, *J. Magn. Magn. Mater,* 1987, **65,** 245.

(2). Lu, A.-H., Schmidt, W., Matoussevitch, N., BPnnermann, H., Spliethoff, B., Tesche, B., Bill, E., Kiefer, W., SchVth, F. (2004) Nanoengineering of a magnetically separable hydrogenation catalyst. *Angew. Chem. Int. Ed. 43,* 4303.

(3). Tsang, S. C., Caps, V., Paraskevas, I., Chadwick, D., Thompsett, D. (2004) Magnetically Separable, Carbon-Supported Nanocatalysts for the Manufacture of Fine Chemicals. *Angew. Chem. Int. Ed. 43,* 5645.

(4). Gupta, A. K., Gupta, M. (2005) Synthesis and surface engineering of iron oxide nanoparticles for biomedical applications. *Biomaterials 26*, 3995.

(5). Li, Z., Wei, L., Gao, M.Y., Lei, H. (2005) One-Pot Reaction to Synthesize Biocompatible Magnetite Nanoparticles. *Adv. Mater. 17*, 1001.

(6). Mornet, S., Vasseur, S., Grasset, F., Verveka, P., Goglio, G., Demourgues, A., Portier, J., Pollert, E., Duguet, E. (2006) Magnetic nanoparticle design for medical applications. *Prog. Solid State Chem. 34*, 237.

(7). Hyeon, T. (2003) Chemical synthesis of magnetic nanoparticles. *Chem. Commun.* 927-934.

(8). Elliott, D.W., Zhang, W. -X. (2001) Field assessment of nanoscale bimetallic particles for groundwater treatment. *Environ. Sci. Technol. 35,* 4922-4926.

(9). Takafuji, M., Ide, S., Ihara, H., Xu, Z. (2004) Preparation of Poly(1-vinylimidazole)-Grafted Magnetic Nanoparticles and Their Application for Removal of Metal Ions *Chem. Mater. 16,* 1977.

(10). Cabrera, L., Gutierrez, S., Menendez, N., Morales, M.P., Herrasti, P. (2008) Magnetite nanoparticles: electrochemical synthesis and characterization. *Electrochim Acta. 53,* 3436.

(11). Pascal, C., Pascal, J. L., Favier, F. (1999) Electrochemical synthesis for the control of $\gamma$-$Fe_2O_3$ nanoparticle size. *Chem Mater. 11,* 141–147.

(12). Bomatí-Miguel, O., Mazeina, L., Navrotsky, A., Veintemillas-Verdaguer, S. (2008) Calorimetric Study of Maghemite Nanoparticles Synthesized by Laser-Induced Pyrolysis. *Chem. Mater. 20,* 591–598.

(13). Wu, W., He, Q., Jiang, C. (2008) Magnetic Iron Oxide Nanoparticles: Synthesis and Surface Functionalization Strategies. *Nanoscale Res Lett. 3,* 397–415.

(14). Babes, L., Denizot, B., Tanguy, G., Jeune, J.J.L., Jallet, P. (1999) Synthesis of Iron Oxide Nanoparticles Used as MRI Contrast Agents: A Parametric Study. *J. Colloid Interface Sci. 212,* 474–482.

(15). Laurent, S., Forge, D., Port, M., Roch, A., Robic, C., Elst, L.V., Muller, R.N. (2008) Magnetic Iron Oxide Nanoparticles: Synthesis, Stabilization, Vectorization, Physicochemical Characterizations, and Biological Applications. *Chem. Rev. 108,* 2064–2110.

(16). Puntes VF, Krishnan KM, Alivisatos AP. Colloidal nanocrystal shape and size control: the case of cobalt. Science. 2001;291(5511):2115–2117. doi: 10.1126/science.1057553.

(17). Park J, Lee E, Hwang NM, Kang MS, Kim SC. et al. One-nanometer-scale size-controlled synthesis of monodisperse magnetic iron oxide nanoparticles. Angew Chem Int Ed. 2005;44(19):2872–2877. doi: 10.1002/anie.200461665.

(18). Nitin N, LaConte LEW, Zurkiya O, Hu X, Bao G. Functionalization and peptide-based delivery of magnetic nanoparticles as an intracellular MRI contrast agent. J Biol Inorg Chem. 2004;9(6):706–712.

(19). Lee SJ, Jeong JR, Shin SC, Kim JC, Chang YH. et al. Nanoparticles of magnetic ferric oxides encapsulated with poly(D,L latide-co-glycolide) and their applications to magnetic resonance imaging contrast agent. J Magn Magn Mater. 2004;272-276:2432–2433.

(20). Akbarzadeh, A., Samiei, M., Davaran, S. Magnetic nanoparticles: preparation, physical properties, and applications in biomedicine. Nanoscale Res. Lett. 2012, 7, 144.

(21). LaConte, L., Nitin, N., Bao, G. (2005) Magnetic nanoparticle probes. *NanoToday 32*.

(22). Wu, W., Dey, D., Memis, O.G., Katsnelson, A., Mohseni, H. (2008) A Novel Self-aligned and Maskless Process for Formation of Highly Uniform Arrays of Nanoholes and Nanopillars. *Nanoscale Res. Lett. 3*, 123-127.

(23). Sahoo, Y., Pizem, H., Fried, T., Golodnitsky, D., Burstein, L., Sukenik, C.N., Markovich, G. (2001) Alkyl phosphonate/phosphate coating on magnetite nanoparticles: A comparison with fatty acids. *Langmuir 17,* 7907–7911.

(24). Lee, H., Lee, E., Kim, D.K., Jang, N.K., Jeong, Y.Y., Jon, S. (2006) Antibiofouling polymer-coated superparamagnetic iron oxide nanoparticles as potential magnetic

resonance contrast agents for in vivo cancer imaging. *J. Am. Chem. Soc. 128,* 7383–7389.

(25). Xu, J., Sun, J., Wang, Y., Sheng, J., Wang, F., Sun, M. (2014) Application of Iron Magnetic Nanoparticles in Protein Immobilization. *Molecules 19,* 11465-11486.

(26). Khot, V.M., Salunkhe, A.B., Phadatare, M.R., Pawar, S.H. (2012) Formation, microstructure and magnetic properties of nanocrystalline Mg-$Fe_2O_4$. *Materials Chemistry and Physics 132*, 782-787.

(27). Katz, E., Willner, I. (2004) Nanobiotechnology: integrated nanoparticle-biomolecule hybrid systems: Synthesis, properties, and applications. *Angew. Chem. Int. Ed. 43,* 6042–6108.

(28). Ferrari, M. (2005) Cancer nanotechnology: Opportunities and challenges. *Nature Rev. Cancer 5,* 161–171.

(29). Arruebo, M., Valladares, M., Gonzalez-Fernandez, A. (2009) Antibody-Conjugated Nanoparticles for Biomedical Applications. *Journal of Nanomaterials 2009,* 1–24.

(30). Yang, J., Lee, C-H., Park, J., Seo, S., Lim, E-K., Song, Y.J., Suh, J-S., Yoon, H-G., Huh, Y-M., Haam, S. (2007) Antibody conjugated magnetic PLGA nanoparticles for diagnosis and treatment of breast cancer. *J. Mater. Chem. 17,* 2695-2699.

(31). Schlenoff, P. (2009) Antibody-coated magnetic nanoparticles: Targeting and treating cancer. *Young Scientists Journal 8,* 33-36.

(32). Bushida, K., Mohri, K., Katoh, T., Kobayashi, A. (1996) Amorphous Wire MI Micro Magnetic Sensor for Gradient Field Detection. *IEEE Trans. Magn. 32*, 4944-4946.

(33). Shinkai, M., Ohshima, A., Yanase, M., Uchiyama, T., Mohri, K., Wakabayashi, T., Yoshida, J., Honda, H., Kobayashi, T. (1998) Development of Novel Magnetic Sensing for Brain Lesion Using Functional Magnetic Particles. *Kagaku Kogaku Ronbunshu 24*, 174-178.

(34). Chan, D.C.F., Kirpotin, D.B., Bunn, P.A. (1993) Synthesis and evaluation of colloidal magnetic iron oxides for the site-specific radiofrequency-induced hyperthermia of cancer. *J. Magn. Magn. Mater. 122,* 374-378.

(35). Roque, A. C. A., Lowe, C. R., Taipa, M. Â. (2004) Antibodies and Genetically Engineered Related Molecules: Production and Purification. *Biotechnol Progress, 20,* 639–654.

(36). Birch, J.R., Racher, A.J. (2006) Antibody production. *Adv Drug Deliv Rev. 58*, 671-85.

(37). Roque, A.C., Silva, C.S., Taipa, M.A. (2007) Affinity-based methodologies and ligands for antibody purification: advances and perspectives. *J Chromatogr A. 1160,* 44-55.

(38). Berensmeier, S. (2007) Magnetic particles for the separation and purification of nucleic acids. *Appl. Micro. Biotech. 73,* 495-504.

(39). Safarik, I., Safarikova, M. (2004) Magnetic techniques for the isolation and purification of proteins and peptides. *Biomagn Res Technol. 2,* 7.

(40). Xu, H., Aguilar, Z.P., Yang, L., Kuang, M., Duan, H., Xiong, Y., Wei, H., Wang, A. (2011) Antibody Conjugated Magnetic Iron Oxide Nanoparticles for Cancer Cell Separation in Fresh Whole Blood. *Biomaterials. 32,* 9758–9765.

(41). Sung, Y.J., Suk, H-J., Sung, H.Y., Li, T., Poo, H., Kim, M-G. (2013) Novel antibody/gold nanoparticle/magnetic nanoparticle nanocomposites for immunomagnetic separation and rapid colorimetric detection of *Staphylococcus aureus* in milk. *Biosens. Bioelectron. 43,* 432–439.

(42). Cui, Y. R., Hong, C., Zhou, Y-L., Li, Y., Gao, X-M., Zhang, X-X. (2011) Synthesis of orientedly bioconjugated core/shell $Fe_3O_4$@Au magnetic nanoparticles for cell separation. *Talanta 85,* 1246–1252.

(43). Chen, S., Yuan, Y., Yao, J., Hana, S., Gu, R. (2011) Magnetic separation and immunoassay of multi-antigen based on surface enhanced Raman spectroscopy. *Chem. Commun. 47,* 4225-4227.

(44). Böttcher, B., Unseld, S., Ceulemans, H., Russell, R.B., Jeske, H. (2004) Geminate structures of *African cassava mosaic virus. J Virol. 78,* 6758-65.

(45). Krupovic, M., Ravantti, J.J., Bamford, D,H. (2009) Geminiviruses: a tale of a plasmid becoming a virus. *BMC Evolutionary Biology 9,* 112.

(46). Zhang, S.C., Wege, C., Jeske, H. (2001) Movement proteins (BC1 and BV1) of Abutilon mosaic geminivirus are cotransported in and between cells of sink but not of source leaves as detected by green fluorescent protein tagging. *Virology. 290,* 249-260.

(47). Swanson, M.M., Valand, G.B., Muniyappa, V., Harrison, B.D. (1998) Serological detection and antigenic variation of two whitefly-transmitted geminiviruses: tobacco leaf curl and croton yellow vein mosaic viruses. *Annals of Applied Biology, 132,* 427–435.

(48). Mohammed Riyaz, S.U., Deepan, S., Dharanivasan, G., Jesse, M.I. Raja Muthuramalingam, T., Kathiravan, K. (2013) First report on a variant of Squash leaf curl China virus (SLCCNV) infecting Benincasa hispida in India. *New Disease Reports 28,* 20.

(49). Czosnek, H., Ber, R., Antignus, Y., Cohen, S., Navot, N., Zamir, D. (1988) Isolation of Tomato Yellow Leaf Curl Virus, a Geminivirus. *Phytopathology. 78,* 508-512.

(50). Vayssieres, L., Chaneac, C., Tronc, E., Jolivet, J.P. (1998) Size tailoring of magnetite particles formed by aqueous precipitation: An example of thermodynamic stability of nanometric oxide particles. *J. Colloid Interf. Sci. 205,* 205-212.

(51). Hu, B., Pan, J., Yu, H.L., Liu, J.W., Xu, J.H. (2009) Immobilization of Serratia marcescens lipase onto amino-functionalized magnetic nanoparticles for repeated use in enzymatic synthesis of Diltiazem intermediate. *Proc. Biochem, 44,* 1019–1020.

(52). Mizukoshi, Y., Shuto, T., Masahashi, N., Tanabe, S. (2009) Preparation of superparamagnetic magnetite nanoparticles by reverse precipitation method: contribution of sonochemically generated oxidants. *Ultrason. Sonochem. 16,* 525–531.

(53). Nedkova, I., Merodiiskaa, T., Slavova, L., Vandenbergheb, R.E., Kusanoc, Y., Takadad, J. (2006) Surface oxidation, size and shape of nano-sized magnetite obtained by co-precipitation. *J. Magn. Magn. Mater. 300,* 358–367.

(54). Qu, S., Yang, H., Ren, D., Kan, S., Zou, G., Li, D., Li, M. (1999). Magnetite nanoparticles prepared by precipitation from partially reduced ferric chloride aqueous solutions. *J. Colloid Interface. Sci. 215,* 190-192.

(55). Pardoe, H., Chua-anusorn, W., Pierre, T.G., Dobson, J. (2001) Structural and magnetic properties of nanoscale magnetic particles synthesised by coprecipitation of iron oxide in the presence of dextran or polyvinyl alcohol. *J. Magn. Mat. 225,* 41–46.

(56). Bandhu, A., Mukherjee, S., Acharya, S., Modak, S., Brahma, S.K., Das, D., Chakrabarti, P.K. (2009) Dynamic magnetic behavior and Mössbauer effect measurements of magnetite nanoparticles prepared by a new technique in the co-precipitation method. *Solid State Commun. 149,* 1790–1794.

(57). Ozkayaa, T., Toprakb, M.S., Baykala, A., Kavasc, H., Koseogluc, Y., Aktas, B. (2009) Synthesis of Fe3O4 nanoparticles at 100ºC and its magnetic characterization. *J. Alloys Compd. 472,* 18–23.

(58). Dellaporta, S.L., Wood, J., Hicks, J.B. (1983) A plant DNA Minipreparation version 2. *Plant Mol. Bio. Rep. 1,* 19-22.

(59). Shi, S.R., Imam, S.A., Young, L., Cote, R.J., Taylor, C.R. (1995) Antigen retrieval immunohistochemistry under the influence of pH using monoclonal antibodies. *J Histochem Cytochem. 43,* 193-201.

(60). Scholten, P.C., Felius, J.A.P. (1990) The magnetical and rheological behavior of aggregating magnetic suspensions. *J. Magn. Magn. Mater.* 85, 107–113.

(61). Cuyper, M.D., Joniau, M. (1991) Mechanistic aspects of the adsorption of phospholipids onto lauric acid stabilized magnetite nanocolloids. *Langmuir, 7,* 647–652.

(62). Wooding, A., Kilner, M., Labrick, B.D. (1992) Stripped magnetic particles. Applications of the double surfactant layer principle in the preparation of water-based magnetic fluids. *J Colloid Interface Sci 149,* 98–104.

(63). Carpenter, E.E., O'Connor, C.J., Harris, V.G. (1999) Atomic structure and magnetic properties of MnFe2O4 nanoparticles produced by reverse micelle synthesis. *J. Appl. Phys. 85,* 5175–5177.

(64). Sousa, M.H., Rubim, J.C., Sobrinho, P.G., Tourinho, F.A. (2001) Biocompatible magnetic fluid precursors based on aspartic and glutamic acid modified maghemite nanostructures. *J. Magn. Magn. Mat. 225,* 67–72.

(65). Canfarotta, F., Piletsky, S.A. (2014) Engineered Magnetic Nanoparticles for Biomedical Applications. *Advanced Healthcare Materials*. 3, 160–175.

(66). Vereda, F., Vicente, J., Hidalgo-Alvarez, R. (2007) Influence of a magnetic field in the formation of magnetite particles via two precipitation methods. *Langmuir 23,* 3581–3589.

(67). Wang, B., Wei, Q., Qu, S. (2013) Synthesis and Characterization of Uniform and Crystalline Magnetite Nanoparticles via Oxidation-precipitation and Modified co-precipitation Methods. *Int. J. Electrochem. Sci., 8,* 3786 – 3793.

(68). Xu, Z.Z., Wang, C.C., Yang, W.L., Deng, Y.H. (2004) Encapsulation of nanosized magnetic iron oxide by polyacrylamide via inverse miniemulsion polymerization. *J Magn. Magn. Mater. 277,* 136-143.

(69). Song, H-T., Choi, J-N., Huh, Y-M., Kim, S., Jun, Y-W., Suh, J-S., Cheon, J. (2005) Surface modulation of magnetic nanocrystals in the development of highly efficient magnetic resonance probes for intracellular labeling. *J. Am. Chem. Soc. 127,* 9992-9993.

(70). Huh, Y-M., Jun, Y-W., Song, H-T., Kim, S., Choi, J-S., Lee, J-H., Yoon, S., Kim, K-S., Shin, J-S., Suh, J-S., Cheon, J. (2005) In Vivo Magnetic Resonance Detection of Cancer by Using Multifunctional Magnetic Nanocrystals. *J. Am. Chem. Soc. 127,* 12387–12391.

(71). Zakri, R.H., Zakri, R., Zakri, S., Hassan, K.U. (2011) Nanotechnology in Surgery: Tiny Solutions for Titanic Problems. *Ann. Pak. Inst. Med. Sci. 7,* 37-41.

(72). Taira, S., Kaneko, D., Onuma, K., Miyazato, A., Hiroki, T., Kawamura-Konishi, Y., Ichiyanagi, Y. (2012) Synthesis and Characterization of Functionalized Magnetic Nanoparticles for the Detection of Pesticide International *J. Inorg. Chem. 2012*.

(73). Cambier, P. Infrared study of goethites of varying crystallinity and particle Size: I. Interpretation of OH and Lattice vibration frequencies. *Clay Minerals,* 1986, **21,** 191-200.

(74). Lerot, L., Low, P.F. (1976) Effect of swelling on the infrared absorption spectrum of montmorillonite. *Clays Clay Miner. 24,* 191-199.

(75). Godbole, B., Badera, N., Shrivastava, S.B., Jain, D., Chandra, L.S.S., Ganesan, V. (2013) Synthesis, Structural, Electrical and Magnetic Studies of Ni- Ferrite Nanoparticles. *Physics Procedia 49,* 2013, 58–66.

(76). Madras, G., McCoy, B.J. (2003) Continuous distribution theory for Ostwald ripening: comparison with the LSW approach. *Chem. Engg. Sci. 58,* 2903 – 2909.

(77). Brusentsov, N.A., Gogosov, V.V., Brusentsova, T.N., Sergeev, A.V., Jurchenko, N.Y., Kuznetsov, A.A., Kuznetsov, O.A., Shumakov, L.I. (2001) Evaluation of ferromagnetic fluids and suspensions for the site-specific radiofrequency-induced hyperthermia of MX11 sarcoma cells in vitro. *J. Magn. Magn. Mater. 225*, 113-117.

(78). Xu, C., Xu, K., Gu, H. Zhong, X, Guo, Z., Zheng, R., Zhang, X., Xu, B. (2004) Nitrilotriacetic acid-modified magnetic nanoparticles as a general agent to bind histidine-tagged proteins. *J. Am. Chem. Soc. 126,* 3392–3393.

(79). Chantrell, R.W., Popplewell, J., Charles, S.W. (1978) Measurements of particle size distribution parameters in ferrofluids. *IEEE Trans. Magn. 14,* 975.

(80). Grabarek, Z., Gergely, J. (1990) Zero-Length Crosslinking Procedure with the Use of Active Esters. *Anal. Biochem. 185,* 131.

(81). Lin, P-C., Chen, S-H., Wang, K-Y., Chen, M-L., Adak, A-K., Hwu, J-R.R., Chen, Y-J., Lin, C-C. (2009) Fabrication of Oriented Antibody-Conjugated Magnetic Nanoprobes and Their Immunoaffinity Application. *Anal. Chem. 81*, 8774–8782.

(82). Packer, L., Tristram, S., Herz, J.M., Russel, C., Borders, L.C. (1979) Chemical modification of purple membranes: role of arginine and carboxylic acid residues in bacteriorhodopsin. FEBS. Lett. 108, 243–248.

(83). Zhou, Y., Rojas, M.R., Park, M-R., Seo, Y-S., Lucas, W. J., Gilbertson, R.L. (2011) Histone H3 Interacts and Colocalizes with the Nuclear Shuttle Protein and the Movement Protein of a Geminivirus. *Journal of Virology, 85*, 11821–11832.

Fig. 1. Schematic representation of the methodology of eluting virion particles using Ab-MNPs.

Fig. 2. a) Particle size analysis data showing that the hydrodynamic diameter of APTES-MNPs at ~25 nm. Inset: Scheme of APTES-MNPs; b) ζ-potential analysis showing the peak at +24.4mV, a net positive charge; c) FT-IR analysis showing peak for A) Bare MNPs, B) APTES-MNPs correnspoding to Fe-O stretch, Si-O bend and N-H bend; d) XRD data showing peaks of bare MNPs compared with APTES-MNPs at (220), (311), (400), (422), (511), (440). e) Hysteresis loop obtained from VSM measurements of synthesized MNPs functionalized with APTES at Room temperature.

Fig. 3. a) ζ-potential analysis data showing increase in the size of the nanoparticles after the immobilization of antibody on magnetic nanoparticles; b) UV-visible spectrophotometer analysis of residual antibody concentration after binding to APTES-MNPs showing reduction in the amount of protein.

Fig. 4. ζ-potential analysis data showing increase in the hydrodynamic diameter of the Ab-MNPs upon addition of virion particles; b) UV-Visible spectrophotometer analysis showing absorbance at ~260nm indicative of unbound protein molecule (impurities); c) SDS-PAGE analysis showing unbound protein (impurities) bands. M-Broad range protein marker, 1 – crude extract from plants, 2-6 showing eluted impure proteins at concentrations 25µL, 50µL, 75µL, 100µL, 125µL respectively; d) Fluorogram of amplification of *CP* gene from the unbound protein molecules showing no amplification in other samples indicative of absence of virion particles in the elute.

Fig. 5. a) SDS-PAGE analysis of virion particles eluted using the antibody-conjugated MNPs showing protein bands at ~85kDa; b) UV-visible spectrophotometer analysis showing elevated peak at ~260nm indicating the presence of protein molecules after elution using Ab-MNPs; c) Fluorogram of amplification of CP gene from the finally eluted sample showing bands at 500bp indicating the presence of virion particles in the elution done using Ab-MNPs.

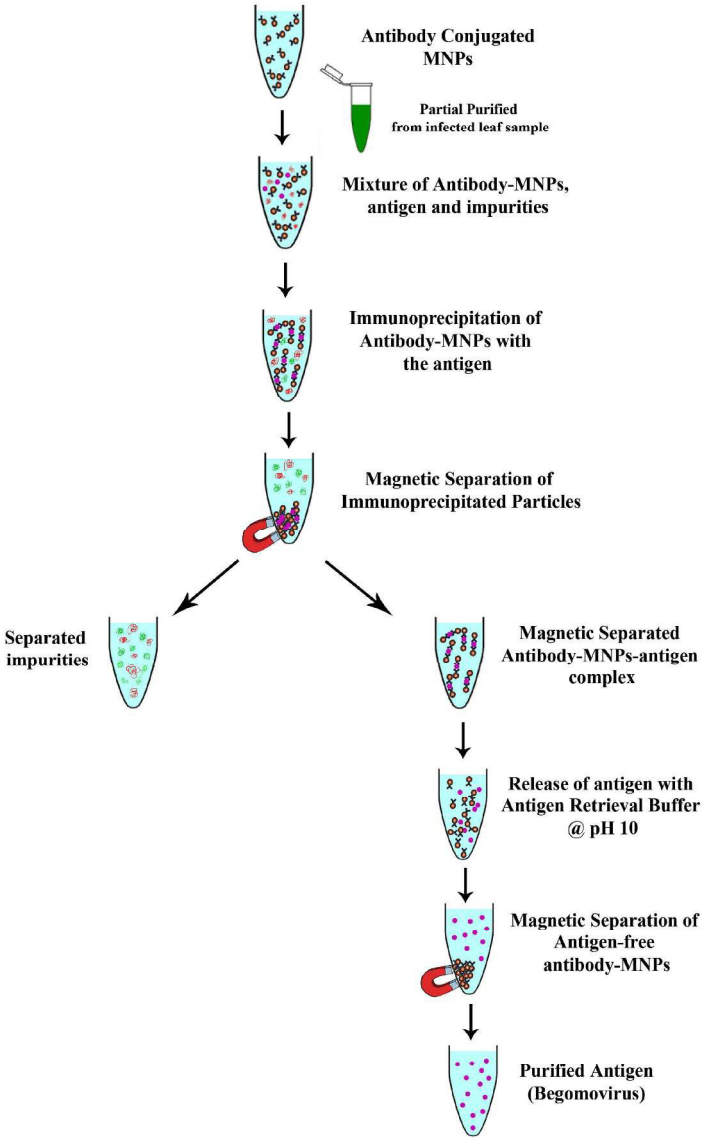


188x308mm (300 x 300 DPI)

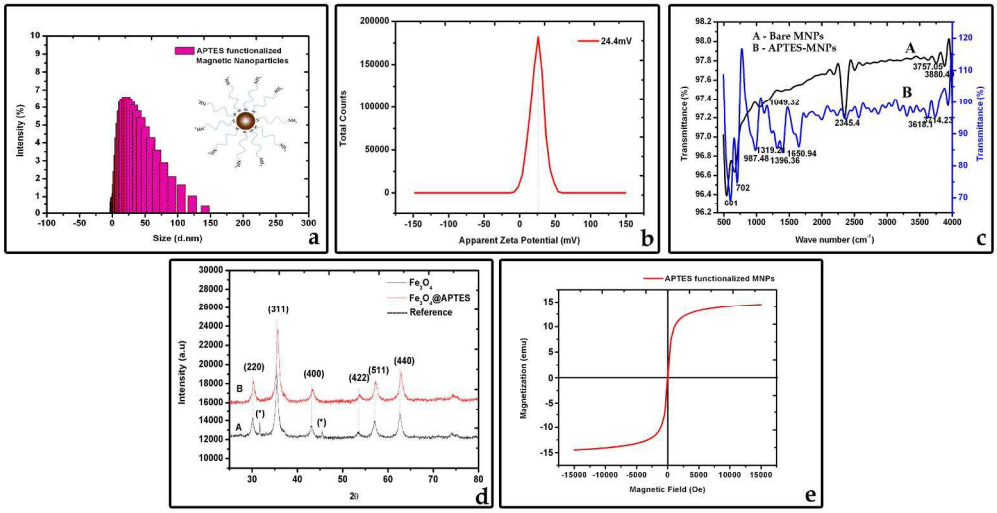


269x139mm (300 x 300 DPI)

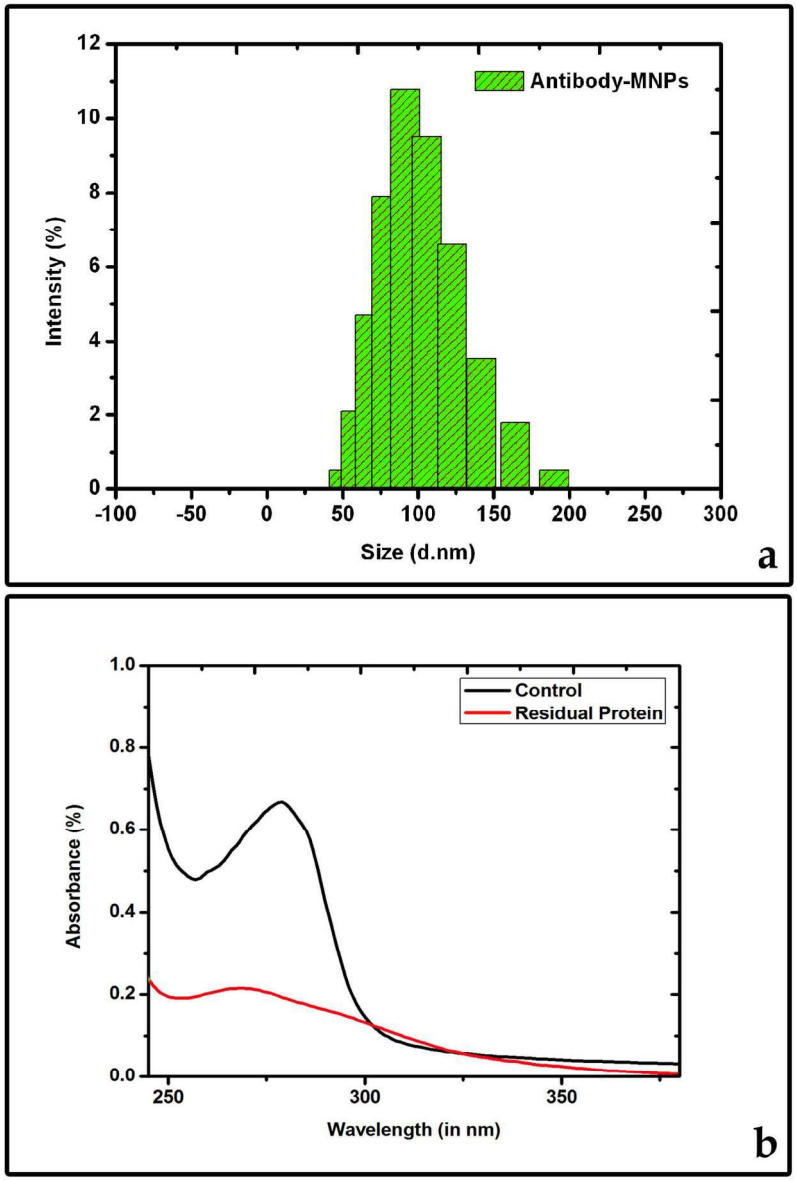


120x178mm (300 x 300 DPI)

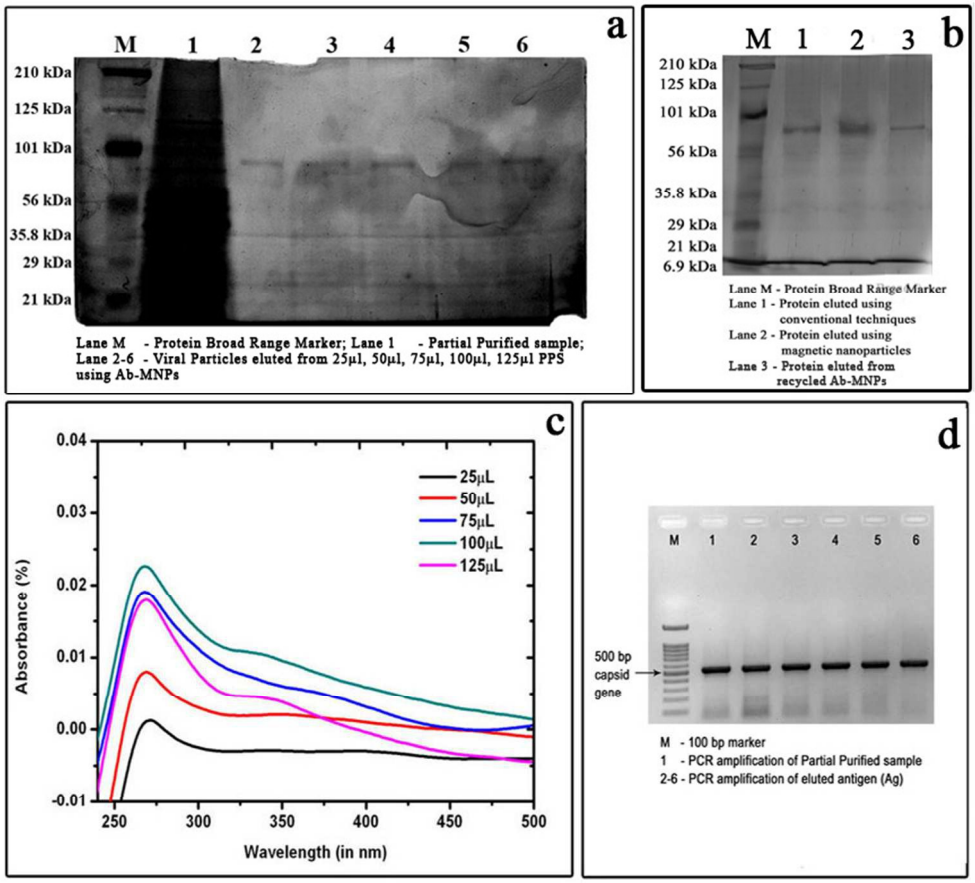


112x102mm (200 x 200 DPI)

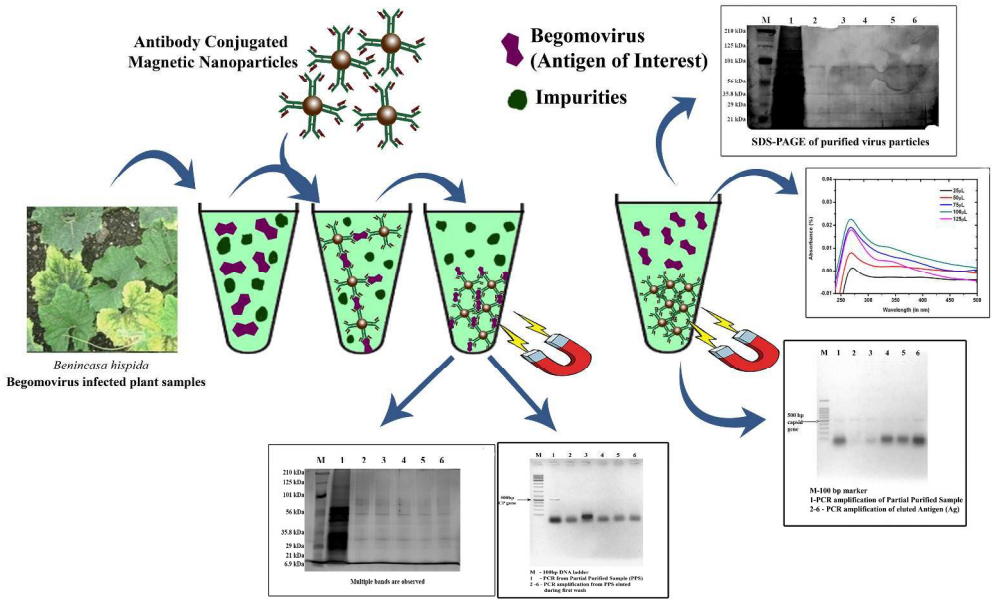


381x254mm (300 x 300 DPI)